ADVANCED COMPOSITES LETTERS

Original Research Article

Advanced Composites Letters
Volume 29: 1–9

DOI: 10.1177/2633366X19899405
journals.sagepub.com/home/acm
SAGE

The parametric instability improvement of fully anisotropic composite plates with embedded shape memory alloy

Zarina Yusof[1], Zainudin A Rasid[1], Mohamad Zaki Hassan[2], SM Sapuan[3], Shamsul Sarip[2], Hafizal Yahaya[1] and Fitri Yakub[1]

Abstract

The parametric resonance or instability challenge in designing laminated composite is crucial in areas such as aeronautical and marine where structures experience dynamic loading. Shape memory alloy (SMA), a type of smart material, has been used to improve the structural behaviours of composite plate using its well-known property of shape memory effect. It is also known that mechanical couplings that exist in unsymmetric composite can increase the instability of the composite. In this study, the SMA property has been exploited to generate recovery stress in the composite to improve its parametric instability problem. The unsymmetric composites were embedded with SMA fibres, and the formulation for the dynamic instability of this composites was developed using finite element method. The third-order shear deformation theory of composite was applied. The results were initially validated for the case of composite without SMA. Following that, the parametric instability behaviour of unsymmetric composites was studied under the effect of several parameters. It was found that the mechanical couplings that exist in the unsymmetric composite have increased the instability of the composite, but the presence of the SMA can significantly reduce this instability.

Keywords

dynamic instability, the Mathieu–Hill equation, laminated composite, shape memory effect

Introduction

Composite material has been widely used in a wide range of industries today[1–3] while shape memory alloy (SMA) has been exploited to improve the composite properties such as fatigue life[4] and its structural behaviours.[5] SMA is a type of smart material that induces stress or strain as its temperature is increased to above a transition temperature called the austenite start temperature. The stress or strain inducement is possible due to the act of one important property of SMA, which is well known as the shape memory effect (SME). Intensive studies on the SMA have been conducted in the past decades in attempts not only to model the SMA characteristics[6,7] but also to apply the SME and other unique properties of the SMA in areas including structural health monitoring,[8] earthquake resistance[9] sports and recreational[10] and medical.[11] Specifically, the SME property of the SMA has been manipulated in the past to improve the structural behaviours of composites including vibration[12] buckling[13–15] and thermal buckling[16] and adaptive structures.[17–19]

[1] Department of Mechanical Precision Engineering, Malaysia-Japan International Institute of Technology, Department of Engineering, Universiti Teknologi Malaysia, Kuala Lumpur, Malaysia
[2] Razak Faculty of Technology and Informatics, Department of Engineering, Universiti Teknologi Malaysia, Kuala Lumpur, Malaysia
[3] Department of Mechanical and Manufacturing Engineering, Advanced Engineering Materials and Composites Research Centre, Universiti Putra Malaysia, Selangor, Malaysia

Date received: 29 July 2019; accepted: 15 December 2019

Corresponding author:
Mohamad Zaki Hassan, Razak Faculty of Technology and Informatics, Department of Engineering, Universiti Teknologi Malaysia, Jalan Sultan Yahya Petra, 54100 Kuala Lumpur, Malaysia.
Email: mzaki.kl@utm.my

Parametric resonance is one type of dynamic instability, indicating its occurrence when a structure shows increasing transverse vibration such that fatigue failure is inevitable if the vibration does not stop.[20] Compared to force resonance that occurs when the excitation frequency coincides with the natural frequency of the structure, parametric resonance can occur at several values of excitation frequency when the structure experiences time varying change in its properties such as stiffness. Parametric instability occurs to all forms of isotropic or anisotropic structures that undergo, among other things, periodic variation of compressive load. The B-spline finite strip method was used in the parametric instability analysis of prismatic plate and laminated composite structures.[21] The first-order shear deformation theory (FSDT) was used to derive the coupled Mathieu equations. The degree of instability of the structure with respect to parameters such as thickness to length ratio and degree of orthotrophy was measured using a dynamic instability index. Sahoo and Singh[22] used the inverse hyperbolic zigzag displacement theory of composite to solve parametric instability of laminated composite and sandwich plates. It was shown that the theory provided more efficient solution to the sought parametric instability chart. Using a refined higher order theory, Babu and Vasudevan[23] conducted parametric instability study on rotating delaminated thickness tapered composite plates, applying the classical laminated plate theory. Yusof and Rasid[24,25] investigated numerically the parametric instability behaviour of composite plates using the FSDT and the third-order shear deformation theory (TSDT) of composite. Parametric instability of composite plates has also been studied in wide variety of other areas such as the variable angle tow composite laminates,[26] laminated composite curved and flat panels subjected to periodic non-uniform in-plane compressive loading[27] and composite panels subjected to area delamination and hygrothermal effect.[28] However, the study on the parametric instability improvement made by smart material such as the SMA, especially on fully anisotropic (unsymmetric) composite structures, can hardly be found in literature.

Tsai and Chen[29] used SMA to enhance the parametric resonance behaviour of composite, but the study was limited to beam structure. Furthermore, several studies were conducted on the effect of symmetric and unsymmetric lamination of the bistable laminated composites.[30] Recently, Roslan et al.[31] published articles on the influence of SMA's active strain energy tuning (ASET) method on the parametric resonance of orthotropic composites using different composite lamination theories. The current study is to further this work on the parametric instability improvement made by SMA, now moving on to fully anisotropic structures. The Mathieu–Hill equation was derived based on the higher order shear deformation theory (HSDT) that includes the warping degree of freedom. By expanding the displacement to include the third-order terms in the warping degree of freedom, the HSDT has the advantage of avoiding to average the transverse shear throughout the composite thickness as it is done for the FSDT and as such more accurate answer can be obtained. The results of instability charts are compared to those of the symmetric composite, and the degree of instability of the unsymmetric composite plate is analysed with regard to several parameters.

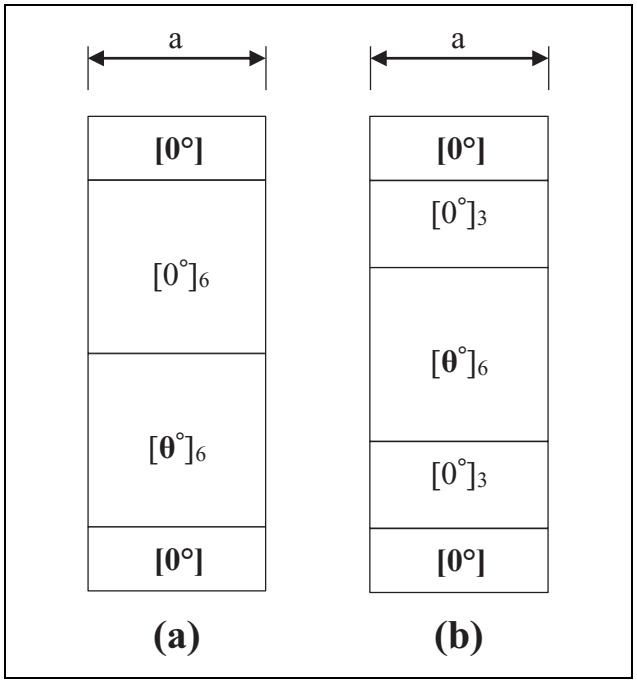

Figure 1. The angle of orientations for (a) unsymmetric and (b) symmetric composites.

Methodology

The material properties of the SMA and the glass–epoxy (GE) composite used here are given in this section. Also, the configurations and dimensions of the laminated composite plates are specified. Following that, the finite element method (FEM) governing equation for the parametric instability problem of the SMA composite plates is derived. The equation is solved through programming codes and flow chart, as shown in Figure 2, which is used in the development of the codes.

Materials

The unsymmetric composite used in this study has the configuration of $[0/0_6/\theta_6/0]$ such as shown in Figure 1(a) where the angle of orientation, θ, can be either 15°, 30°, 45°, 75° or 90°.[32] The outer layers with 0° angle of orientation are the SMA-epoxy (SE) layers (darkened in Figure 1) while GE are the constituent of other layers. The 0° for the SE layers refers to the direction of the SMA fibres, while for other layers, the angle is for the direction of glass fibres.

Table 1. Material properties of the composite.[23]

Material	Young's modulus, E (GPa)	Shear modulus, G (GPa)	Poisson's ratio, v
Glass fibre	65.50	120.63	0.23
Epoxy	3.43	1.27	0.35
Nitinol	$E_m = 33.0$ $E_a = 69.6$	$G_m = 33.0$ $G_a = 69.6$	0.33

Table 2. Parameters of the SMA for the Brinson model.[27]

Parameters	Values
Critical stress start, $\sigma_{cr,s}$ (Pa)	80 (10^6)
Critical stress finish, $\sigma_{cr,f}$ (Pa)	155 (10^6)
Martensite Young's modulus, E_M (Pa)	33 (10^9)
Austenite Young's modulus, E_A (Pa)	69.6 (10^9)
Maximum residual strain, ε_L	0.058
Initial strain, e	0.001
Martensite finish temperature, M_f (°C)	20.7
Martensite start temperature, M_s (°C)	26.8
Austenite start temperature, A_s (°C)	37.2
Austenite finish temperature, A_f (°C)	47.0
Stress influence coefficient, C_A (Pa °C^{-1})	10.6 (10^6)
Stress influence coefficient, C_M (Pa °C^{-1})	9.7 (10^6)

SMA: shape memory alloy.

For comparison purpose, symmetric composites having the configuration of $[0/0_3/\theta_6/0_3/0]$, as shown in Figure 1(b), are also analysed. The square plate used in this study has side dimensions of $a = b = 500$ mm. The ratio of length over thickness, a/t, is specified for each case study. The boundary condition used throughout the study is pin supported at both ends of the plate.

The SMA used in this study is the nickel–titanium alloy, better known as Nitinol. The material properties of the glass fibre, epoxy and Nitinol are given in Table 1. The subscript 'm' refers to martensite phase of Nitinol at low temperature, while the subscript 'a' refers to austenite phase of Nitinol at high temperature. The prediction of the recovery stress, σ_r, and the Young's modulus, E_s, of Nitinol as it is heated to a certain activation temperature, T_a, was done using the Brinson model.[27]

Table 2 gives the properties of the SMA along with the related parameters needed for the application of the Brinson model. The parameters of critical stress start, $\sigma_{cr,s}$, and critical stress finish, $\sigma_{cr,f}$, are the stress values needed for the beginning of the reorientation process of the SMA at low temperature below Martensite finish temperature, M_f, where with the addition of stress, SMA reoriented itself from temperature-induced martensite to stress-induced martensite (detwinned martensite). This is one of the improved features added in the Brinson model from the earlier models of Tanaka[33] and Liang and Rogers[34] where with this addition, the quasi-plasticity[35] behaviour of SMA at low temperature is considered. Furthermore, with the given parameters, the maximum residual strain of $\varepsilon_L = 0.058$ can be obtained if the stress in the stress-induced martensite form of SMA is released after reaching, $\sigma_{cr,f}$.

Table 3. Tensile strength (σ_r) and Young's modulus (E_s) of the SMA based on the Brinson model at $T_a = 55°$.[27]

ε_0 (m/m)	0.001	0.003	0.005	0.008	0.01
E_s (GPa)	68.82	55.1	49.28	44.93	43.2
σ_r (MPa)	86.49	118.84	128.53	135.95	139.08

SMA: shape memory alloy.

Solving the Brinson model at certain temperature, T_a, and the SMA initial strain, ε_0, the σ_r and E_s of the SMA were obtained as given in Table 3. As an example, with pre-strain of $\varepsilon_0 = 0.001$ given to SMA before it is embedded into layers of laminated composite plate, the Brinson model predicts that the recovery stress that can be induced within the SMA is $\sigma_r = 86.49$ MPa. In addition, with the thermoelastic transformation occurring from martensite to austenite, the new improved Young's modulus of the SMA is $E_s = 68.82$ GPa. The increase of these two values are the reason for the parametric instability improvement of the laminated composite plate in this study.

The Mathieu–Hill equation

The Mathieu–Hill equation is derived here using FEM according to the TSDT. Following that, the Mathieu–Hill equation is solved using the Bolotin's method to obtain the eigenvalue equations that determine the instability charts of the SMA composite plates. The effective properties of the SE layer and the GE layer were derived using the rule of mixture. A perfect bonding is assumed between SMA and matrix. For example, through the rule of mixture, the Poison's ratio, v

$$\nu_{12} = \nu_n V_n + \nu_{12e} V_e \tag{1}$$

and the shear modulus in two-direction, i

$$E_2 = \frac{E_{2e} E_n}{V_e E_n + V_n E_{2e}} \tag{2}$$

The displacement field of the SMA-laminated composite plate is assumed to be as stated below[32]

$$\begin{aligned} u(x,y,z,t) &= u_0(x,y,t) + z\theta_x(x,y,t) + z^3\xi_x \\ v(x,y,z,t) &= v_0(x,y,t) + z\theta_y(x,y,t) + z^3\beta \\ w(x,y,z,t) &= w_0(x,y,t) \end{aligned} \tag{3}$$

where u_0, v_0 and w_0 are the midplane displacements in x, y and z directions, respectively. The rotations in the x-z plane is θ_x while θ_y is rotation in the y-z plane. ξ_x and ξ_y are variables representing warping in the x-z and y-z

planes, respectively. Furthermore, strains can be expressed as

$$\{\varepsilon\} = \begin{Bmatrix} \varepsilon_x \\ \varepsilon_y \\ \gamma_{xy} \end{Bmatrix} = \begin{Bmatrix} \dfrac{\partial u_0}{\partial x} \\ \dfrac{\partial v_0}{\partial y} \\ \dfrac{\partial u_0}{\partial y} + \dfrac{\partial v_0}{\partial x} \end{Bmatrix} + z \begin{Bmatrix} \dfrac{\partial \theta_x}{\partial x} \\ \dfrac{\partial \theta_y}{\partial y} \\ \dfrac{\partial x}{\partial y} + \dfrac{\partial \theta_y}{\partial x} \end{Bmatrix} + z^3 \begin{Bmatrix} \dfrac{\partial \xi_x}{\partial x} \\ \dfrac{\partial \theta_y}{\partial y} \\ \dfrac{\partial \xi_x}{\partial y} + \dfrac{\partial \theta \xi_y}{\partial x} \end{Bmatrix} \tag{4}$$

or

$$\{\varepsilon\} = \{\varepsilon_m\} + z\{\varepsilon_s\} + z^3\{\varepsilon_w\} \tag{5}$$

where $\{\varepsilon_m\}$ is the in-plane vector of strain, $\{\varepsilon_s\}$ is the flexural vector of strain and $\{\varepsilon_w\}$ is the warping vector of strain. The transverse shear strain vector is

$$\{\gamma\} = \begin{Bmatrix} \gamma_{xz} \\ \gamma_{yz} \end{Bmatrix} = \begin{Bmatrix} \dfrac{\mathrm{d}w}{\mathrm{d}x} + \theta_x + 3z^2\xi_x \\ \dfrac{\mathrm{d}w}{\mathrm{d}y} + \theta_y + 3z^2\xi_y \end{Bmatrix} \tag{6}$$

Applying the standard FEM procedures and conforming to the Hamilton's principle such as

$$\int_{t_1}^{t_2} \left(\delta \left[\int \sigma_{ij}\varepsilon_{ij} \mathrm{d}V \right] - \delta \int \dot{a}\rho\dot{a} \mathrm{d}V - \delta W \right) \mathrm{d}t = 0 \tag{7}$$

the parametric instability equation for composite plate with embedded SMA is

$$[M]\{\ddot{q}\} + ([K_\mathrm{L}] + [K_\mathrm{s}] + [K_\mathrm{r}])\{q\} + P(t)[K_\mathrm{G}]\{q\} = 0 \tag{8}$$

where $[M]$ is the mass matrix, $[K_\mathrm{L}]$ is the linear stiffness matrix, $[K_\mathrm{s}]$ is the shear stiffness matrix, $[K_\mathrm{r}]$ is the recovery stress of the SMA stiffness matrix and $[K_\mathrm{G}]$ is the geometric stiffness matrix. $P(t)$ is the periodic external load that can be represented to consist of static part, P_s, and dynamic part, P_t, such as

$$P_\mathrm{s} = \alpha P_{cr} \ , \ P_t = \beta P_{cr} \tag{9}$$

where P_cr is the critical (buckling) load of the plate and α is the static load factor while β is the dynamic one. Equation (8) is converted to the Mathieu–Hill equation such as

$$\begin{aligned} &[M]\{\ddot{q}\} + ([K_\mathrm{L}] + [K_\mathrm{s}] + [K_\mathrm{r}])\{q\} \\ &\quad -(\alpha P_\mathrm{cr}[K_\mathrm{G}] - \beta P_\mathrm{cr}[K_\mathrm{G}]\cos\omega t)\{q\} = 0 \end{aligned} \tag{10}$$

In Bolotin's method of solution, it is assumed that the solution of $\{q\}(t)$ is a series, for a period of T such as

$$\{q\} = \frac{1}{2}\{b_o\} + \sum_{i=2,4.}^{\alpha} \left[\{a\}_i \sin\left(\frac{i\omega t}{2}\right) + \{b\}_i \cos\left(\frac{i\omega t}{2}\right) \right] \tag{11}$$

Inserting equation (11) into equation (8) and equating coefficients for sin(ωt) and cos(ωt) terms, the solution to equation (10) is

$$\left[[K] - \alpha P_\mathrm{cr}[K_\mathrm{G}] \pm \frac{1}{2}\beta P_\mathrm{cr}[K_\mathrm{G}] - \frac{\omega^2}{4}[M] \right]\{q\} = 0 \tag{12}$$

In this work, equation (12) divides dynamic instability region into lower and upper stability boundaries by knowing the values of α, β and P_cr. To solve equation (12), linear buckling analysis needs to be conducted to determine the $[K_\mathrm{G}]$ and P_cr while the mass matrix $[M]$ also needs to be determined. Furthermore, equation (12) was solved using the developed source codes, and the flow chart of the codes is given in Figure 2.

Results and discussion

The formulation and codes are firstly validated based on past results. The effects of several parameters on the parametric resonance of the unsymmetric composite were investigated.

Validation

As data related to parametric resonance of unsymmetric composite are limited in the literature, the validation of the codes has been done on symmetric composite. Parametric instability analysis has been conducted on a composite with symmetric cross-ply configuration of [0/90/90/0]. Rectangular plate was used where side length is 500 mm. The a/t ratio is 25. Table 4 represents that the non-dimensionalised frequency values obtained in this investigation agreed closely with results from various methods of finite strips[35] and FEM.[12] It shows here that with a rather simple addition of warping terms in the displacement field equations of the present HSDT model, the results obtained are in excellent agreement with the results coming from more complicated models or formulations in the work of Wang and Dawe,[21] Zak et al.[38] and Chakrabarti and Sheikh.[39]

Furthermore, the presently developed formulation based on the HSDT can be seen in Figure 3 to agree strongly with the FSDT-based formulation developed by Zak et al..[38] In this study, the activation temperature (T_act) is equal to 55°

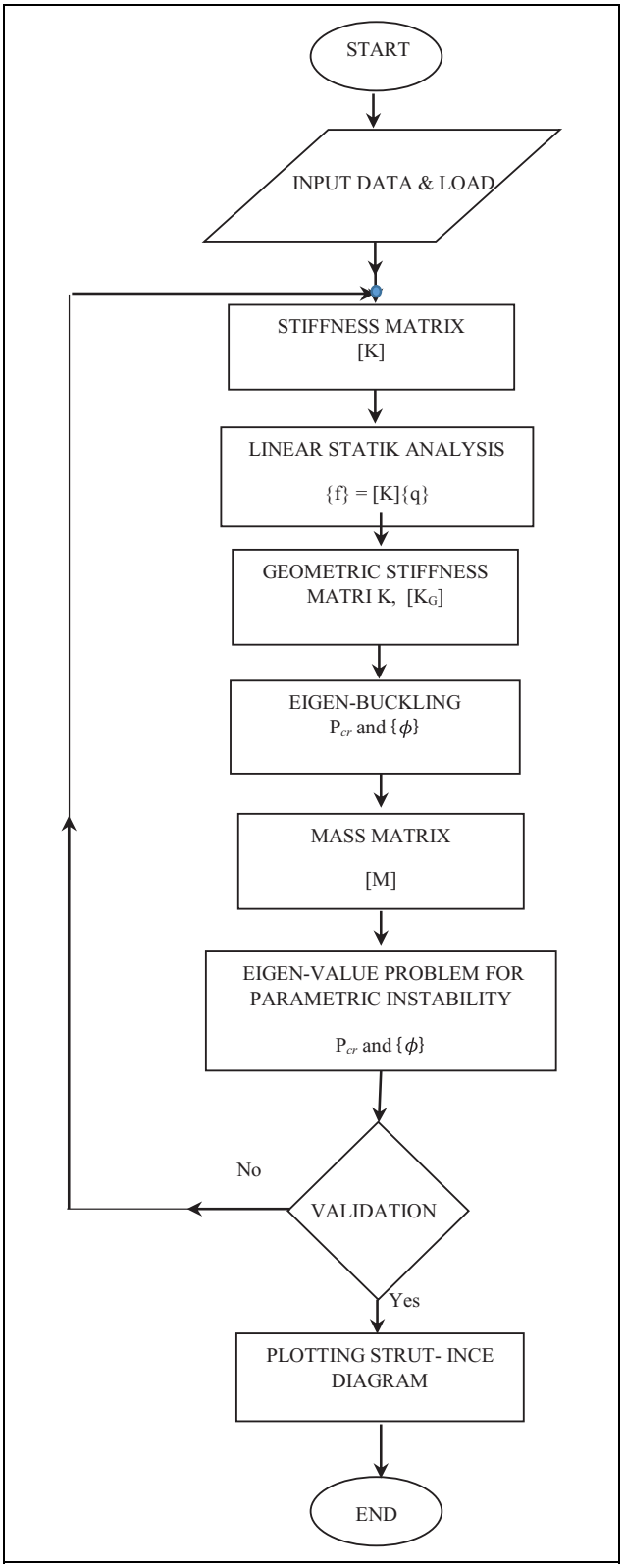

Figure 2. The flow chart for the source codes.

while the initial strain (ε_o) is 0.01, and through the Brinson model, the recovery stress induced (σ_r) is equal to 139.8 MPa while the SMA Young's modulus is 43.3 GPa. Furthermore, WO is the case of the composite without SMA, while WS is the case of the composite with the addition of SMA. It shows that using the HSDT, accurate results can be obtained without having to estimate the shear effect of thickness using the shear correction factor as in the FSDT. Furthermore, the induction of the recovery stress and the increase of the Young's modulus with the addition of SMA into composite can be seen to greatly improve the parametric instability behaviour of the composite by shifting the frequency centre to the right. The non-dimensionalised frequency centre (frequency at $\beta = 0$) can be seen to shift from 15.363 to 28.92, an increase of about 88%. Furthermore, the trend of this finding is in close agreement with the results for FSDT-based formulation developed by Chakrabarti and Sheikh.[39] In contrast, Pradyumna and Bandyopadhyay[40] observed that the origin of instability regions obtained by the HSDT formulation has higher excitation frequency parameters than the corresponding value for the FSDT formulation. The origin of instability regions offered a higher excitation frequency with increasing width of dynamic instability regions, possibly due to the increase of shell stiffness and curvature.[41]

The effect of the mechanical coupling

To study the effect of the mechanical couplings on the dynamic instability of SMA composite plates, four configurations of laminated composite were used where the first two configurations are the 12-layer symmetric composite, $[0_3/\theta_6/0_3]$ (S12L), and unsymmetric composite, $[0_6/\theta_6]$ (US12L). The unsymmetric composite here is known to give mechanical coupling as opposed to the first symmetric configuration of composite, as studied by Lagace et al.[32] who studied buckling of unsymmetric composite laminates. The other two configurations are the 14-layer symmetric, $[0/0_3/\theta_6/0_3/0]$ (S14L), and unsymmetric composites, $[0/0_6/\theta_6/0]$ (US14L), where the outer 0° layer is for the embedment of SMA fibres. The study was conducted on rectangular composite plate with aspect ratio, $a/b = 0.5$, while the ratio of length to thickness is $a/t = 25$. The SMA, having 0.008 m/m as initial strain, is heated to activation temperature, $T_a = 55$°C to give $\sigma_r = 135.95$ MPa and $E_s = 44.93$ GPa, which are listed in Table 3. Figure 4 shows that the presence of mechanical couplings can greatly increase the instability of the composite plate. This can be seen by the frequency centre (frequency at $\beta = 0$) of the instability chart that is moved to the left from 52.635 of the S12L composite to 37.367 of the US12L composite, which is a decrease of about 29%. Similarly, in a study by Birman[42] while applying an analytical method, it was found that the frequency centre shifted to the left when the composite was changed to unsymmetric composite. This was especially true for composite plates with large aspect ratio. The instability of the unsymmetric composite can be seen to greatly improve when the 0° layers are simply added to the top and bottom layers of the composite. The effect of

Table 4. The validation on the developed formulation and source codes.

		Present HSDT		Wang and Dawe[21]		Sahoo and Singh[36]		Kao et al.[37]	
α	β	Ω^U	Ω^L	Ω^U	Ω^L	Ω^U	Ω^L	Ω^U	Ω^L
0	0	144.485	144.485	144.57	144.57	144.546	144.546	144.36	144.36
0	0.3	154.943	133.209	155.03	133.29	155.008	133.264	155.64	133.79
0	0.6	164.739	120.885	164.83	120.95	164.807	120.936	165.12	121.45
0	0.9	173.983	107.153	174.08	107.21	174.056	107.198	174.43	107.63
0	1.2	182.761	91.381	182.87	91.43	182.837	91.419	183.21	91.86
0	1.5	191.136	72.243	191.25	72.28	191.216	72.273	191.75	72.62
0.2	0.06	131.632	126.785	131.71	126.86	131.687	126.838	132.12	127.26
0.4	0.12	117.381	106.175	117.45	106.24	117.429	106.219	117.96	106.82
0.6	0.18	101.140	80.446	101.20	80.48	101.182	80.480	101.84	81.10
0.8	0.24	81.733	40.867	81.78	40.89	81.767	40.884	82.31	41.32

HSDT: higher order shear deformation theory. Ω^U: Upper frequency, Ω^L: Lower frequency.

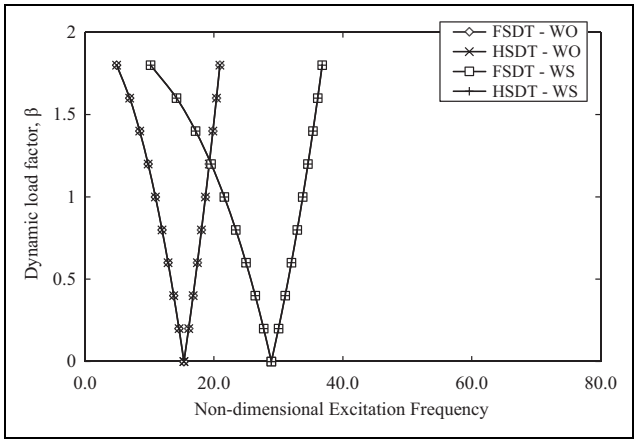

Figure 3. The comparison between the instability charts correspond to the present HSDT and the FSDT. HSDT: higher order shear deformation theory; FSDT: first-order shear deformation theory; WO: composite without shape memory alloy; WS: composite with shape memory alloy.

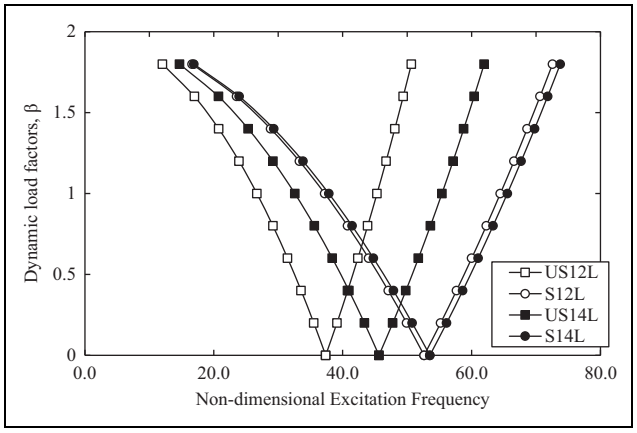

Figure 4. The comparison between the instability charts correspond to the symmetric and unsymmetric composite in the case of WO. WO: composite without shape memory alloy.

adding the outer 0° layers seems to be unaffected in the case symmetric composites. This finding agrees well with the previous work of the same author.[13]

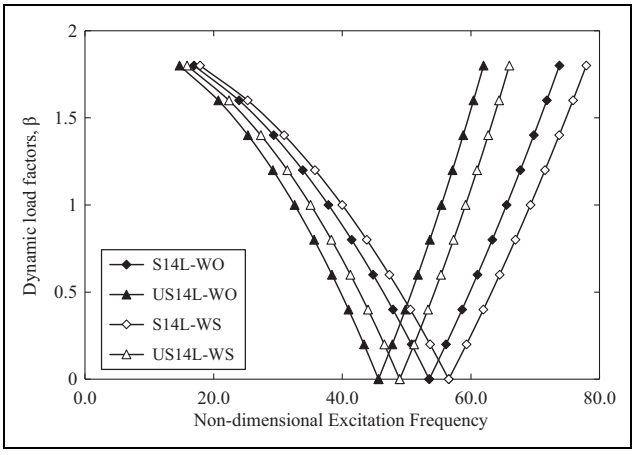

Figure 5. The comparison between the instability charts correspond to the symmetric and unsymmetric composites in the case of WO and WS. WO: composite without shape memory alloy; WS: composite with shape memory alloy.

The effect of SMA on the parametric instability of unsymmetric composite can be seen in the study conducted on the 14-layer composite plates with and without SMA. Figure 5 shows that the unsymmetric composite plate, US14L-WO, shows higher instability than its symmetric counterpart, S14L-WO. It can be seen that the shifting of frequency centre is from 53.524 to 45.632, a decrease of about 15%. However, with the addition of SMA fibres at the outer layers of the composite in US14L-WS, the instability chart is seen to move to the right to give an improvement to its parametric instability state. This is consistent with the effect of SMA that shift the post-buckling path of composite plates to the right[42] and also shifting instability chart of composite beams.[29] In addition, Park et al.[41] mentioned that the natural frequencies of the plate with SMA are lower than those of the plate without SMA fibre due to the increase of the weight of plate and decrease of the thermal large deflection. They evaluated the vibration behaviour of the composite plate embedded with SMA fibres that is studied using the FEM based on the FSDT.

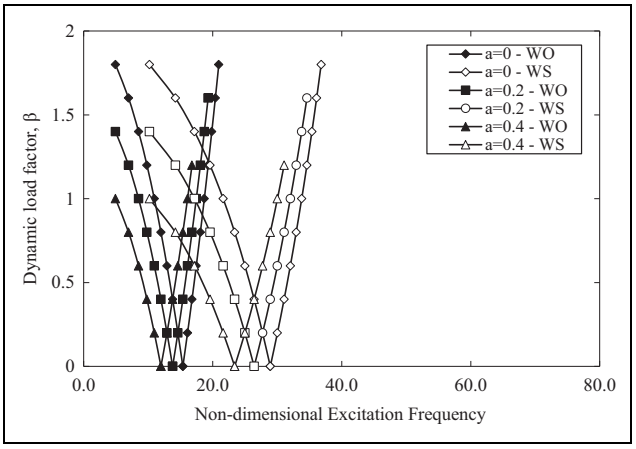

Figure 6. The effect of the static load factor, α (a) on the dynamic instability of unsymmetric composites. WO: composite without shape memory alloy; WS: composite with shape memory alloy.

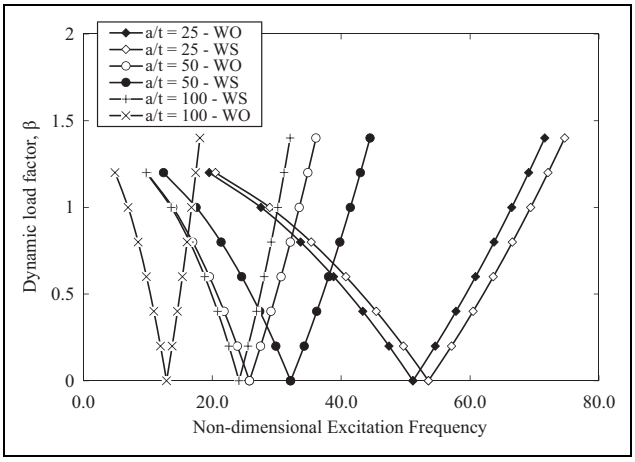

Figure 7. The instability charts of composite plates for WS and WO cases having different a/t ratios. WS: composite with shape memory alloy; WO: composite without shape memory alloy.

The optimal design has the design variable as the SMA fibre angle, stacking sequence, volume fraction and initial strain of the SMA filter should be performed in order that SMA is applied to the structures effectively.

The static load factor effect

The unsymmetric composite used in this part of study has a configuration of $[0/0_6/90_6/0]$. The ratio of length to thickness is $a/t = 100$. Figure 6 shows the instability charts of the unsymmetric composites for different values of static instability factor, α (a). It shows that as α is increased, the frequency centre and the instability chart move to the left for both cases of composite without SMA (WO) and composite with SMA (WS). This means that the instability is increased as α is increased. At the same time, the width of the instability chart also increases as α is increased. This also means that as α is increased, the instability of the composite plates is increased as the instability region is increased. A study by Sahoo and Singh[22] on the dynamic instability of sandwich composite plate found similar behaviour where the onset of instability regions occurs earlier with wider instability region for the gradual increase of static load factor. The effect of SMA with the addition of the recovery stress can be seen to obviously improve the instability of the composite by shifting the instability chart to the right. However, the region of instability increases at the same time with the addition of the SMA to the composite as α is increased. It can thus be said that the ASET effect of the SMA improves the parametric instability of unsymmetric composites merely by postponing the onset of instability region but at the same time does not improve the instability through reduction of area of instability that is due to the increase of α. This is in line with the finding for the effect of SMA on symmetric composite, as stated by Yusof et al.[43] This inability of the SMA can be improved if the sources of recovery stress such as the initial strain, activation temperature and the volume fraction of the SMA are increased. In the study by Tsai and Chen,[29] the increase of initial strain, activation temperature and volume fraction of SMA was seen to not only increase the frequency centre of the instability chart but also decrease the region of instability.

The length to thickness ratio effect

In this section, the effect of thickness of SMA composite plate with $[0/0_6/90^\circ{}_6/0]$ configuration is studied by varying the a/t ratio of the composite plate. The SMA with initial strain of $\varepsilon_0 = 0.005$ is activated at $T_a = 55^\circ$C to give $\sigma_r = 128.53$ MPa and $E_s = 49.28$ GPa, based on the Brinson model simulation (see Table 3). Figure 7 shows the plots of instability charts for different a/t values correspond to the case of composite without SMA (WO) and composite embedded with SMA (WS). The plot shows the instability decreases as the thickness is increased for both cases of WO and WS. This can be seen when the instability charts are shifted to the right as thickness is increased. However, the width of the instability chart can be seen to increase as the thickness is increased. Similar effect can be seen for the case of orthotropic plates.[31] An interesting finding for the case of sandwich structure is when the thickness of the core with respect to the thickness of face is increased, not only the centre of frequency is shifted to the left but also the region of instability is increased. The SMA had a greater influence on thinner composite plates where the amount of jump of the frequency centre to the right is much higher than those of the thicker plate where at $a/t = 25$, the effect of SMA can be seen to be very small. This higher influence of SMA on thinner plate can be seen in the problem of static

instability problem,[42] natural frequency[43] and critical buckling.[44–46]

Conclusions

The investigation on the parametric instability of unsymmetric composite plates with embedded SMA was performed using FEM. The development of the parametric resonance equation was done based on the HSDT of composite. Validation analysis conducted showed that the developed formulation and codes gave accurate results compared to past results. Several studies were performed to investigate the effect of several parameters on the parametric instability of unsymmetric SMA composite plates. It was found that as the mechanical coupling increases, the parametric instability of composite plates was increased as the chart shifted to the left, and the addition of SMA to the composite is capable of decreasing the instability by shifting the charts back to the right.

Acknowledegement

Appreciation is given to Universiti Teknologi Malaysia and Ministry of Higher Education under Fundamental Research Grant Scheme, Industry International Incentive Grant and 'Geran Universiti Penyelidik' (GUP) Tier 2 for financial support provided throughout the course of this research project. They also thank Ministry of Education Malaysia and Universiti Putra Malaysia for the financial support through the Visiting Scholar (Post-Doctoral) scholarship.

Declaration of conflicting interests

The author(s) declared no potential conflicts of interest with respect to the research, authorship, and/or publication of this article.

Funding

The author(s) disclosed receipt of the following financial support for the research, authorship, and/or publication of this article: This work was supported by Universiti Teknologi Malaysia and Ministry of Higher Education under Fundamental Research Grant Scheme, R.K.130000.7840.4F880, Industry International Incentive Grant Q.K.130000.3043.01M46 and 'Geran Universiti Penyelidik' (GUP) Tier 2, Q.K.130000.2656.17J66.

ORCID iD

Mohamad Zaki Hassan https://orcid.org/0000-0002-2321-0604

References

1. Radzi A, Sapuan S, Jawaid M, et al. Effect of alkaline treatment on mechanical, physical and thermal properties of roselle/sugar palm fiber reinforced thermoplastic polyurethane hybrid composites. *Fibers Polym* 2019; 20: 847–855.
2. Atiqah A, Jawaid M, Sapuan S, et al. Thermal properties of sugar palm/glass fiber reinforced thermoplastic polyurethane hybrid composites. *Compos Struct* 2018; 202: 954–958.
3. Hassan MZ, Sapuan S, Roslan SA, et al. Optimization of tensile behavior of banana pseudo-stem (*Musa acuminate*) fiber reinforced epoxy composites using response surface methodology. *J Mater Res Technol* 2019; 8: 3517–3528.
4. Abdy AI, Hashemi J and Al-Mahaidi R. Fatigue life improvement of steel structures using self-prestressing CFRP/SMA hybrid composite patches. *Eng Struct* 2018; 174(1): 358–372.
5. Ali A, Antonietta LCA, Biffi CA, et al. Cohesive surface model for delamination and dynamic behavior of hybrid composite with SMA-GFRP interface. *Int J Lightweight Mater Manuf* 2019; 2(2): 146–155.
6. Liang C and Rogers C. One-dimensional thermomechanical constitutive relations for shape memory materials. *J Intel Mat Syst Str* 1997; 8: 285–302.
7. Brinson L and Lammering R. Finite element analysis of the behavior of shape memory alloys and their applications. *Int J Solids Struct* 1993; 30: 3261–3280.
8. Bielefeldt BR, Hochhalter JD and Hart DJ. Shape memory alloy sensory particles for damage detection: experiments, analysis, and design studies. *Struct Health Monit* 2018; 17(4): 777–814.
9. Nunes P and Lobo PS. Influence of the SMA constitutive model on the longitudinal seismic response of RC bridges. *Procedia Struct Integrity* 2019; 17: 624–631.
10. Mohd Jania J, Learya M, Subica A, et al. A review of shape memory alloy research, applications and opportunities. *Mater Des* 2014; 56: 1078–1113.
11. Lv C, Su Q, Fang J, et al. Styrene-maleic acid copolymer-encapsulated carbon monoxide releasing molecule-2 (SMA/CORM-2) suppresses proliferation, migration and invasion of colorectal cancer cells in vitro and in vivo. *Biochem Biophys Res Commun* 2019; 520(2): 320–326.
12. Zhang Z and Sheng P. Research on stability and nonlinear vibration of shape memory alloy hybrid laminated composite panel under aerodynamic and thermal loads. *J Intell Mater Syst Struct* 2016; 27: 2851–2861.
13. Rasid ZA, Mazlan SA, Amran A, et al. The strain energy tuning of the shape memory alloy on the post-buckling of composite plates using finite element method. *Adv Mater Res* 2012; 445: 577–582.
14. Hassanli S and Samali B. Buckling analysis of laminated composite curved panels reinforced with linear and nonlinear distribution of Shape Memory Alloys. *Thin-Walled Struct* 2016; 106: 9–17.
15. Rasid ZA, Amran A, Zahari R, et al. Thermal buckling and post-buckling improvements of laminated composite plates using finite element method. *Key Eng Mat* 2011; 471: 536–541.
16. Asadi H, Kiani Y, Aghdam M, et al. Enhanced thermal buckling of laminated composite cylindrical shells with shape memory alloy. *J Compos Mater* 2016; 50: 243–256.
17. Chillara VSC and Dapino MJ. Shape memory alloy-actuated bistable composites for morphing structures. In: Hani E (ed.), *Behavior and mechanics of multifunctional materials and composites XII*, Vol. 10596. *International Society for Optics and Photonics*, 2018, Bellingham, Washington, USA: Naguib. p. 1059609.

18. Hufenbach W, Gude M and Kroll L. Design of multistable composites for application in adaptive structures. *Compos Sci Technol* 2002; 62(16): 2201–2207.
19. Daynes S, Potter KD and Weaver PM. Bistable prestressed buckled laminates. *Compos Sci Technol* 2008; 68(15–16): 3431–3437.
20. Bolotin V. *Dynamic stability of elastic systems*. EI Segundo: Aerospace Corporation, 1962.
21. Wang S and Dawe D. Dynamic instability of composite laminated rectangular plates and prismatic plate structures. *Comput Methods Appl Mech Eng* 2002; 191: 1791–1826.
22. Sahoo R and Singh B. Dynamic instability of laminated composite and sandwich plates using a new inverse hyperbolic zigzag theory. *J Aerospace Eng* 2014; 28: 04014109.
23. Babu AA and Vasudevan R. Dynamic instability analysis of rotating delaminated tapered composite plates subjected to periodic in-plane loading. *Arch Appl Mech* 2016; 86: 1965–1986.
24. Yusof Z and Rasid ZA. Numerical modelling of parametric instability problem for composite plate using finite element method. *AIP Conf Proc* 2016; 1750: 030044.
25. Yusof Z and Rasid ZA. Parametric instability of laminated composite plates using third order shear deformation theory. *Adv Sci Lett* 2017; 23: 4434–4438.
26. Samukham S, Raju G and Vyasarayani C. Parametric instabilities of variable angle tow composite laminate under axial compression. *Compos Struct* 2017; 166: 229–238.
27. Ovesy H and Fazilati J. Parametric instability analysis of laminated composite curved shells subjected to non-uniform in-plane load. *Compos Struct* 2014; 108: 449–455.
28. Panda H, Sahu S and Parhi P. Hygrothermal response on parametric instability of delaminated bidirectional composite flat panels. *Euro J Mech-A/Solids* 2015; 53: 268–281.
29. Tsai XY and Chen LW. Dynamic stability of a shape memory alloy wire reinforced composite beam. *Compos Struct* 2002; 56: 235–241.
30. Chillara VSC and Dapino MJ. Stability considerations and actuation requirements in bistable laminated composites. *Compos Struct* 2018; 184: 1062–1070.
31. Roslan S, Yusof Z, Rasid ZA, et al. Dynamic instability response of smart composite material. *Mater Werkst* 2019; 50: 302–310.
32. Lagace PA, Jensen DW and Finch DC. Buckling of unsymmetric composite laminates. *Compos Struct* 1986; 5: 101–123.
33. Tanaka K. A phenomenological description on thermomechanical behavior of shape memory alloys. *J Press Vessel Technol (Trans ASME)* 1990; 112: 158–163.
34. Liang C and Rogers C. One-dimensional thermomechanical constitutive relations for shape memory materials. *Journal of Intelligent Material System and Structure* 1990; 1: 207–1234.
35. Seelecke S and Muller I. Shape memory alloy actuators in smart structures: modeling and simulation. *Appl Mech Rev* 2004; 57: 23–46.
36. Sahoo R and Singh B. Dynamic instability of laminated-composite and sandwich plates using a new inverse trigonometric zigzag theory. *J Vib Acoust* 2015; 137: 061001.
37. Kao JY, Chen CS and Chen WR. Parametric vibration response of foam-filled sandwich plates under periodic loads. *Mech Compos Mater* 2012; 48: 525–538.
38. Zak A, Cartmell M and Ostachowicz W. Dynamics of multilayered composite plates with shape memory alloy wires. *J Appl Mech* 2003; 70(3): 313–327.
39. Chakrabarti A and Sheikh AH. Behavior of laminated sandwich plates having interfacial imperfections by a new refined element. *Comput Mech* 2004; 34(2): 87–98.
40. Pradyumna S and Bandyopadhyay JN. Dynamic instability of functionally graded shells using higher-order theory. *J Eng Mech* 2009; 136(5): 551–561.
41. Park JS, Kim JH and Moon SH. Vibration of thermally post-buckled composite plates embedded with shape memory alloy fibers. *Compos Struct* 2004; 63: 179–188.
42. Birman V. Dynamic stability of unsymmetrically laminated rectangular plates. *Mech Res Commun* 1985; 12: 81–86.
43. Yusof Z, Rasid ZA, Hassan MZ, et al. Parametric study on dynamic instability of fully anisotropic composite plates. *Int J Eng Technol* 2018; 7: 132–136.
44. Rasid ZA, Zahari R and Ayob A. The instability improvement of the symmetric angle-ply and cross-ply composite plates with shape memory alloy using finite element method. *Adv Mech Eng* 2014; 6: 632825.
45. Rasid ZA. The natural frequency of the shape memory alloy anti-symmetric angle-ply composite plates using finite element method. *Appl Mech Mater* 2015; 695: 52–55.
46. Rasid ZA and Yahaya H. The thermal instability analysis of functionally graded carbon nanotube composite plates using finite element method. *Appl Mech Mater* 2015; 695: 285–288.